

# First results with a microcavity plasma panel detector

R. Ball<sup>a</sup>, M. Ben-Moshe<sup>c</sup>, Y. Benhammou<sup>c</sup>, R. Bensimon<sup>c</sup>,  
J. W. Chapman<sup>a</sup>, M. Davies<sup>c</sup>, E. Etzion<sup>c</sup>, C. Ferretti<sup>a</sup>, P. S. Friedman<sup>d</sup>,  
D. S. Levin<sup>a</sup>, Y. Silver<sup>c</sup>, R. L. Varner<sup>b</sup>, C. Weaverdyck<sup>a</sup>, B. Zhou<sup>a</sup>

<sup>a</sup> *University of Michigan, Department of Physics, Ann Arbor, Michigan, 48109, USA.*

<sup>b</sup> *Oak Ridge National Laboratory, Physics Division, Oak Ridge, Tennessee, 37831, USA.*

<sup>c</sup> *Tel Aviv University, School of Physics and Astronomy, Tel Aviv, Israel.*

<sup>d</sup> *Integrated Sensors, LLC, Ottawa Hills, Ohio, 43606, USA.*

---

## Abstract

A new type of gaseous micropattern particle detector based on a closed-cell microcavity plasma panel sensor is reported. The first device was fabricated with  $1 \times 1 \times 2$  mm cells. It has shown very clean signals of 0.6 to 2.5 volt amplitude, fast rise time of approximately 2 ns and FWHM of about 2 ns with very uniform signal shapes across all pixels. From initial measurements with beta particles from a radioactive source, a maximum pixel efficiency of greater than 95% is calculated, for operation of the detector over a 100V wide span of high voltages (HV). Over this same HV range, the background rate per pixel was measured to be 3 to 4 orders of magnitude lower than the rate with the cell illuminated by the beta source. Pixel-to-pixel count rate uniformity is within 3% and stable within 3% for many days. The time resolution is 2.4 ns, and a very low cell-to-cell crosstalk has been measured between cells separated by 2 mm.

*Keywords:* micropattern gas detector; particle detector; plasma panel sensor.

---

## 1. Introduction

Plasma panel sensors (PPS) with *open*-cell structures as particle radiation detectors have been investigated by our group for several years [1]. The first results for a new radiation detector based on a *closed*-cell microcavity-PPS structure are here described. This research aims at developing scalable, inexpensive, low mass, long life and hermetically sealed gaseous detectors for both scientific and commercial applications.

The panel acts as an array of independent closed gas pixels/cells biased to discharge when free-electrons or ions are generated in the gas by ionizing radiation. The electron avalanche is self-contained by the walls that define the cell itself and suppressed using Penning mixtures [2] with quenching gases and a localized resistance at each pixel. The HV applied to each pixel is chosen such that the mode of operation is in the Geiger region [3], and rendering this device intrinsically digital. The cell capacitance, which was measured to be  $0.3 \pm 0.1$  pF, stores the total charge available for a pulse.

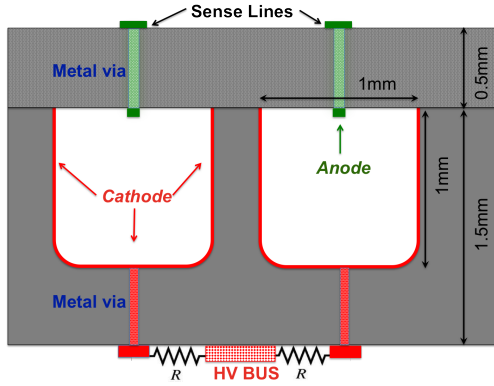


Figure 1: Concept side view of a microcavity-PPS panel.

The detector consists of two substrates (see Fig. 1) sealed together. The top supports the anode in each cell, which is connected by a metal via to a readout (RO) or sense line on the outside. The bottom hosts the metalized cavities, each one with a metal via connecting the cathode to the HV distribution by means of an external quench resistor. In this first prototype, cells of  $1 \times 1 \times 2$  mm were arranged with a low packing fraction of 18% as shown in Fig. 2. Smaller cells with much higher packing fractions are planned for the next generation of detectors.

## 2. Experimental Results

### 2.1. Setup and DAQ

The gas used for the experiments described here was 1 atm of Argon-Neon Penning mixture with  $\text{CF}_4$  added to improve the response with and without a radioactive source. Each pixel was instrumented with a  $1\text{G}\Omega$  quench resistor. The response was investigated with a  $^{106}\text{Ru}$   $\beta$ -emitter source.

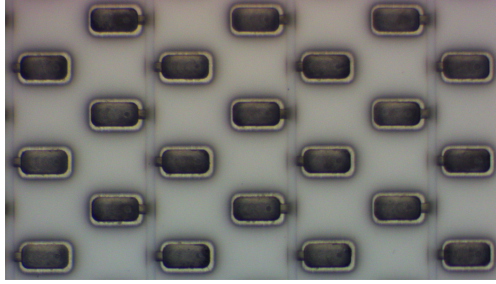


Figure 2: Photograph of part of a microcavity-PPS bottom substrate with  $1 \times 1 \times 2$  mm metalized microcavity array. Three thin gas lines (vertical) are visible, each servicing two columns of cavity pixels.

In most of the tests the readout signals were first discriminated before being sent to a Wiener NIMbox, configured as a 20 channels scaler using customized firmware, readout by locally developed LabVIEW code.

For efficiency and time resolution measurements, the coincidence of an external pair of scintillator detectors was used to generate a trigger for the readout, using 20 ns wide, NIM logic signals. The coincidence window of the panel and trigger was  $2 \mu\text{s}$ .

In order to acquire the signal time spectrum, a portable version of the LHC ATLAS precision muon chambers readout system called MiniDAQ [4] is used. This system is capable of recording integrated charge and times relative to the trigger with 0.78 ns precision.

## 2.2. Signal response

The signal produced by a discharge is very clean ( $S/N > 20$ ), has a range of amplitudes from 600 mV (at HV=800V) to 2.5 V (at HV=1200V) requiring no amplification electronics, and has rise times of about 2 ns and FWHM of between 2 to 3 ns, as shown in Fig. 3.

Fig. 4 shows the hit rate of a single pixel, exposed to the collimated source, as a function of the applied high voltage. A plateau between 1090V and 1190V is clearly visible. Over the whole range of HV tested, less than 0.01 Hz of background per pixel were measured whereas with the source, a count rate of 2 to 3 orders of magnitude higher was observed. Data taken with an uncollimated source shows that a single pixel can count at rates up to 400 Hz or more (at higher voltages) maintaining a very low background with a 3 to 4 orders of magnitude source to background ratio.

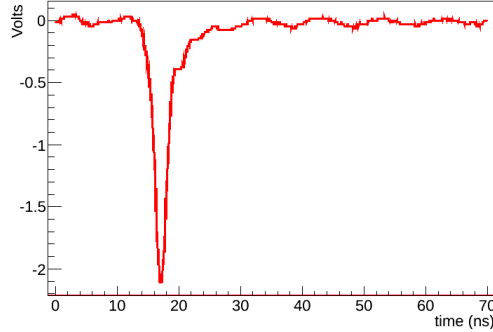


Figure 3: Example of microcavity-PPS pulse operating at 1150V.

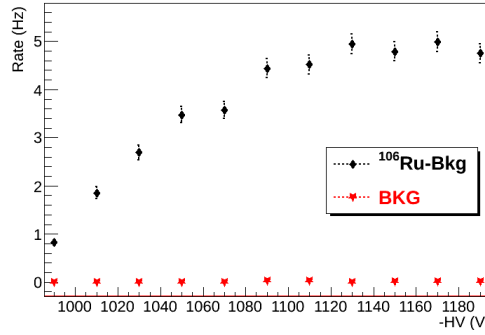


Figure 4: Single microcavity-PPS pixel rate response to  $^{106}\text{Ru}$  at different HV.

### 2.3. Pixel uniformity

The response rates of different pixels was measured to determine the quality of the parts and their assembly. Fig. 5 shows a histogram of the rate at fixed voltage of pixels illuminated by the collimated  $^{106}\text{Ru}$  source. The distribution has a variance of about 12% over 52 pixels tested (see Fig. 5).

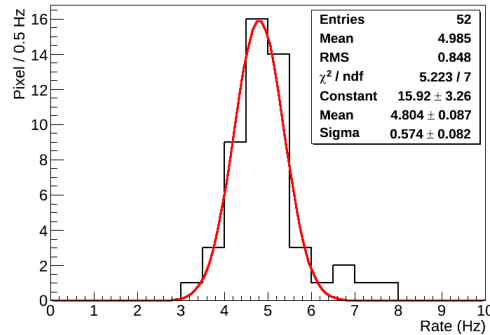


Figure 5: Histogram of microcavity-PPS single cell response rates to a collimated  $^{106}\text{Ru}$  source at 1050V for 52 pixels. The distribution is fitted with a Gaussian function.

A more precise measurement of the pixel response uniformity was obtained by exposing the detector to a source placed at a distance far away enough to produce an approximate uniform flux of radiation over the whole panel. The rate measured on each readout line was proportional to the number of pixels instrumented on that line (Fig. 6). The RMS variation was about 3%, smaller than the variance determined from Fig. 5. The difference is largely due to alignment errors in placing the collimator on each pixel.

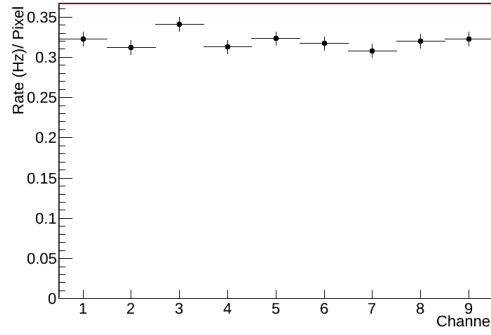


Figure 6: Microcavity-PPS response rate exposed to an uncollimated  $^{106}\text{Ru}$  source 13 cm above the panel. The RMS on the Y-axis is 3%.

#### 2.4. Pixel isolation

The pixel isolation was directly confirmed by the result shown in Fig. 7. This plot displays the hit map associated with the collimated  $^{106}\text{Ru}$  source placed over a single pixel in readout (RO) line #6, in a configuration that had 21 other active cells nearby.

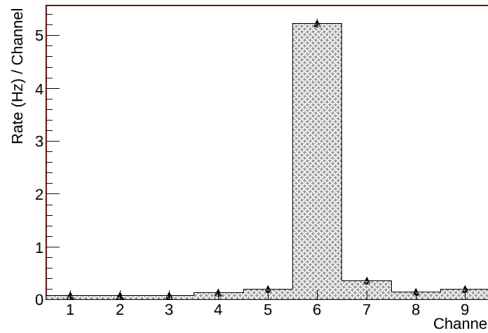


Figure 7: Hit map of the microcavity-PPS with 22 active pixels (not all the lines have the same number of pixels) and where a  $^{106}\text{Ru}$  source was collimated over a pixel on RO #6.

The measured rate on the illuminated line was significantly larger than the one on the other lines which remained very close to the background level, confirming that a pixel discharge on one line does not affect the others. The slightly higher observed rate on the two lines adjacent to the illuminated is due to the collimator diameter being slightly larger than the cell, which leads to a small collateral leakage contribution to the neighbors.

### 2.5. Time stability

Fig. 8 exhibits the stability of the pixel response rate in time: the plot is the average hourly count rate under the uncollimated  $^{106}\text{Ru}$  source placed 15 cm above the panel. The first 18-20 hours show a fast change in response rate due to the individual gas components still mixing (i.e., the DAQ was started immediately after filling the panel one gas component at the time). After this period, the RMS variation was  $\sim 3\%$  over the next 9 days.

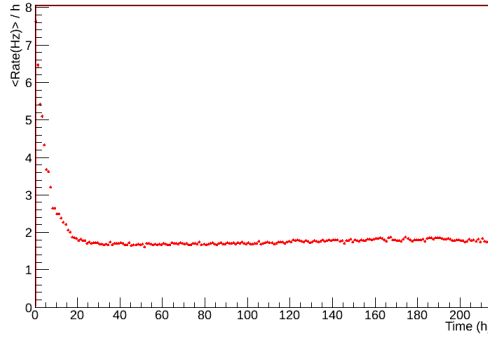


Figure 8: Microcavity-PPS single pixel response as a function of time at 1000V.

### 2.6. Efficiency

The pixel efficiency is defined as the ratio of the number of events with a coincidence between a pulse in the microcavity pixel and a trigger, divided by the total number of triggers. The calculation of the efficiency was corrected using GEANT4 [5] mainly because of two effects that increased the number of triggers: 1) the collimator diameter was larger than 1 mm, causing a fraction of the source  $\beta$ 's to trigger an event even when not passing through the pixel. 2) triggers due to secondary electrons from X-rays produced by the  $^{106}\text{Ru}$   $\beta$ 's interacting either in the panel substrates or in the scintillators. The trigger rate was also measured with a plate identical to the collimator but without the hole: roughly one third of the triggers are recorded in this

configuration. This data driven method of subtracting the fraction of triggers coming from the source and not going through the pixel active area reduced the dependence of the result on simulation.

Fig. 9 shows the pixel efficiency measured as a function of the applied HV for two pixels. The fit lines, based on a Fermi-Dirac function, each show a plateau, one at  $\varepsilon \sim 95\%$  and another at  $\varepsilon \sim 100\%$ . The total systematic error was estimated to be about 10%, and was due to a misalignment between the collimated source and the pixel, and the pixel relative to the trigger.

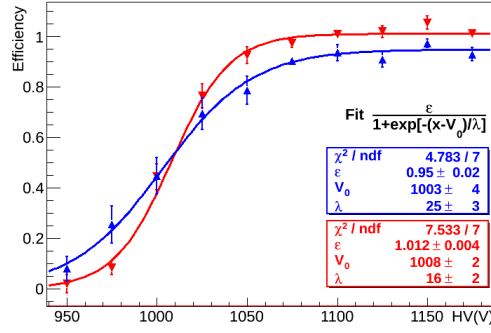


Figure 9: Microcavity-PPS pixel efficiency as a function HV measured for two pixels.

### 2.7. Time resolution

The response time of single pixel hits from the collimated  $^{106}\text{Ru}$  source is shown in Fig. 10, where the number of hits is plotted as a function of the pulse arrival time after subtraction (event by event) of the trigger time.

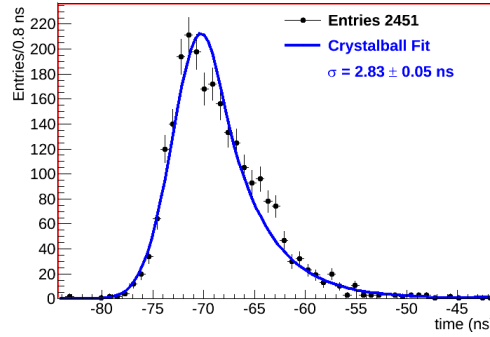


Figure 10: Distribution of the microcavity-PPS single cell arrival time at 1530V.

The experimental points were fitted with a Crystal Ball function, a convolution of a Gaussian with a power law accounting for an asymmetric tail [6].

The Gaussian part of the distribution reflects the stochastic nature in which the avalanche leads to the discharge, while the tail represents the longer drift times of electrons arriving from regions with lower field and farther away from the anode. The time resolution, defined as the dispersion in the time difference between the pixel signal threshold crossing and the trigger time, shown by the Gaussian sigma of the fit is  $\sim 2.8$  ns. This width includes the trigger jitter, measured at 1.5 ns. The approximate procedure of subtraction in quadrature of the trigger component yields a Gaussian time resolution of 2.4 ns. The distribution's negative mean was due to a lack of correction for the trigger delay with respect to the pulse (e.g. extra cables, electronics, etc.).

### 3. Summary

The microcavity-PPS detector prototype showed very promising results in terms of pixel-to-pixel uniformity and time-stability of both signal shape and rates. The prototype has also demonstrated very low background over a wide range of applied high voltages, excellent pixel response isolation, time resolutions of a few nanoseconds, and efficiencies above 95% over a 100 volt range for beta particles emitted by a  $^{106}\text{Ru}$  radioactive source.

The geometrical parameters of the panel microcavity cell design can be tuned for specific applications including smaller cells and much higher packing fractions. These changes, together with the optimization of the gas mixture and reduced quench resistances, could increase the maximum response rate, improve both the spatial and time resolution, and increase the overall efficiency. Based on these initial results, the development of this technology should provide a promising alternative for particle detection.

### Acknowledgements

Development of the PPS project was funded by the U.S. Department of Energy (DOE) - Office of Nuclear Physics Small Business Innovation Research grant award numbers de-sc0006204 and DE-FG02-07ER84749 to Integrated Sensors, LLC; U.S. DOE, Office of Nuclear Physics, Applications of Nuclear Science and Technology grant to Oak Ridge National Laboratory, operated by UT-Battelle, LLC for the U.S. DOE; and DOE - Office of High Energy Physics grant number DE-FG02-12ER41788 to the University of Michigan. The research at Tel Aviv University was supported by the I-CORE



Program of the Planning and Budgeting Committee and the Israel Science Foundation (grant number 1937\12). Funding for scientific exchange and collaboration between Tel Aviv University and the University of Michigan was provided by the Israel-American Binational Science Foundation, grant number 1008123.

Disclaimer: This report was prepared as an account of work sponsored by an agency of the United States Government. Neither the United States Government nor any agency thereof, nor any of their employees, makes any warranty, express or implied, or assumes any legal liability or responsibility for the accuracy, completeness, or usefulness of any information, apparatus, product, or process disclosed, or represents that its use would not infringe privately owned rights. Reference herein to any specific commercial product, process, or service by trade name, trademark, manufacturer, or otherwise does not necessarily constitute or imply its endorsement, recommendation, or favoring by the United States Government or any agency thereof. The views and opinions of authors expressed herein do not necessarily state or reflect those of the United States Government or any agency thereof.

## References

- [1] R. Ball et al., “Development of a Plasma Panel Radiation Detector”, Nucl. Inst. & Meth. Phys. Res. A 764 (2014) 122-132
- [2] M.J. Druyvesteyn and F.M. Penning “The Mechanism of Electrical Discharges in Gases of Low Pressure” Rev. Mod. Phys. 12 (1940) 87 [Erratum *ibid.* 13 (1941) 72].
- [3] Glenn F. Knoll “Radiation Detection and Measurement”, fourth edition, ISBN: 978-0-470-13148-0.
- [4] Y.Arai *et al.*, “ATLAS Muon Drift Tube Electronics” 2008 JINST 3 P09001, <http://iopscience.iop.org/1748-0221/3/09/P09001>
- [5] S. Agostinelli *et al.*, “Geant4a simulation toolkit”, Nuclear Instruments and Methods in Physics Research Section A: Accelerators, Spectrometers, Detectors and Associated Equipment Volume 506, Issue 3, 1 July 2003, Pages 250-303
- [6] RooFit <http://root.cern.ch/root/html/RooCBSShape.html>